Thin Solid Films 689 (2019) 137493

Contents lists available at ScienceDirect

Thin Solid Films

journal homepage: www.elsevier.com/locate/tsf

Mitigating early fracture of amorphous metallic thin films on flexible substrates by tuning substrate roughness and buffer layer properties

Hai T. Tran[a], Truong Do[b], Wenjun Cai[c,*]

[a] Department of Mechanical Engineering, University of South Florida, 4202 E. Fowler Avenue, Tampa, FL 33620, USA
[b] Department of Industrial Engineering, University of Louisville, 132 Eastern Pkwy, Louisville, KY 40292, USA
[c] Department of Materials Science and Engineering, Virginia Polytechnic Institute and State University, 460 Old Turner Street, Blacksburg, VA 24061, USA

ARTICLE INFO

Keywords:
Amorphous thin film
Flexible substrate
Interface adhesion
J-integral
Finite element analysis

ABSTRACT

Ductility mismatch between brittle amorphous thin films and flexible polymer substrate often leads to limited elongation and early failure of the system. A combined experimental and computational study was carried out to investigate the roles of buffer layer material type, thickness, and substrate roughness on the fracture toughness of the amorphous thin film/polymer system. Experimentally, about 1 μm thick amorphous aluminum-manganese thin films were deposited on polyimide substrates and tested in tension. The reliability of such systems was found to be strongly influenced by the film/substrate interface adhesion. Several strategies to improve the adhesion of the interface were conducted, including roughening the surface of the substrate, and adding a buffer layer with a desired mechanical properties and thickness. Computationally, finite element simulations of the same system were carried out under tension. It was found that by introducing substrate roughness and adding a Cr buffer layer of 75 nm, the interface toughness of the film/substrate can be increased by almost twenty times. The results of the present work may shed light on the interfacial engineering strategies for improving reliability of future flexible electronics.

1. Introduction

In flexible electronic devices, the dramatic mechanical property (e.g. ductility, stiffness, and strength) mismatch between the rigid metal and semiconductor thin films and the stretchy and compliant substrate often leads to early failure of the system. The situation is even worse when the film is of a brittle nature, e.g. amorphous magnetic material [1], metallic glass [2,3], and some alloy films produced by non-equilibrium processes such as electrodeposition and physical vapor deposition [4]. Compared to ductile metallic materials, many brittle thin films have been proven to be outstanding candidates as functional materials due to their good magnetic properties [5,6], excellent corrosion resistance [7–9], and metallic bonding ability [10–12]. While some brittle films exhibit high elastic limit (~3–4%) [13], their early fracture is mainly due to the lack of intrinsic crack propagation barriers such as grain boundaries or secondary phase boundaries for further strain hardening beyond the elastic limit. When elongated, the brittle film fails to co-deform with the flexible substrate up to high strains. Hence ameliorating this situation is critical for ensuring reliable performance of future flexible electronic devices.

Past research show that the film/substrate interface property strongly affects the ductility and fracture resistance of the overall system. It was found that improved adhesion delayed the interface debonding [14,15], and retarded strain localizations such as shear band formation and necking, resulting in a large failure strain [14–18]. On the other hand, if the metallic film delaminates from the substrate because of weak adhesion, the support from the substrate is lost. The film then becomes freestanding and tends to form a neck, resulting in failure at a small strain (typically below 1%) [14,16,17,19]. To increase the toughness, the interface can be engineered to release the stresses to the adjacent layer, resulting in a smaller probability of delamination [20–22]. Various strategies have been applied to enhance the film/substrate interface adhesion, such as increasing interface roughness, adjusting the thickness of the buffer layer, etc. [23–28]. Despite recent progresses, most of these studies has focused on a single buffer layer type (e.g. Cr or Cu) without clear justification of the selection of the material type or its thickness. Such considerations have motivated the authors to combine both experimental and computational study aiming to answer the following question: what combination of buffer layer type (soft vs. hard, brittle vs. ductile), thickness, and substrate roughness leads to be best fracture toughness of the system. Specifically, two strategies were investigated here, including 1) roughening the surface

* Corresponding author.
E-mail address: caiw@vt.edu (W. Cai).

https://doi.org/10.1016/j.tsf.2019.137493
Received 13 January 2019; Received in revised form 23 July 2019; Accepted 7 August 2019
Available online 07 August 2019

of the polymer substrate, and 2) adding a buffer layer and then tuning its thickness. In this work, two buffer layer material were investigated: Al and Cr, representing a soft (and ductile) and strong (and brittle) material respectively. The buffer layer thickness was varied from 20 to 100 nm. Selection of this range of thicknesses was motivated by previous studies where a metallic buffer layer of ~ 20–100 nm was found to significantly enhance interfacial adhesion between Ta/polyimide (PI) and Cu/PI [25,29].

In the present work, the investigated system is a ~1.2 μm thick Al-Mn alloy thin film magnetron sputtered on 7.6 μm thick PI substrate. The ductility and crystallinity of the film can be tuned by varying Mn concentration in the alloy, as shown in our previous work [4]. A chemically homogenous, amorphous phase was obtained with 20.5 at.% Mn addition, confirmed by energy dispersive spectra. Using a similar procedure described before [4], tensile tests of monolithic Al-Mn alloy coated on PI were performed to obtain the mechanical properties of the system. Such properties were then used as inputs in the finite element simulations to evaluate the fracture resistance of the system by varying the substrate roughness and/or the buffer layer material property and thickness.

2. Materials and method

2.1. Materials synthesis, characterization, and testing

The PI substrate (Kapton HN by DuPont, 7.6 μm thick) roughness was introduced by oxygen plasma etching (Plasma-Therm PECVD/RIE system) under 50 cc/s of oxygen flow, 2666.5 Pa (or 20 Torr) process pressure and 35 W of RF power for 120 s in reactive ion etching (RIE) mode. The roughness R_a (i.e. arithmetic average of absolute values of surface profile) was ~100 nm, measured by Dektak D150 profiler. Note that the roughness of the intact PI substrate was measured to be < 20 nm (averaged from three separated measurements). On either smooth or rough PI substrate (~7.6 μm), a single buffer layer, either Al or Cr, with layer thicknesses of 20, 50, 75 and 100 nm was deposited prior to the deposition of Al-Mn films. Al-20.5 at.% Mn (hereafter referred as Al-Mn for simplicity) thin films (~1.2 μm) was then deposited on top of the buffer layer by magnetron sputtering following procedures described before [4].

Microstructure of as-deposited samples was characterized using high resolution transmission electron microscopy (HRTEM) and selected area diffraction (SAD). Transmission electron microscopy (TEM) samples were prepared by directly sputtering the Al-Mn alloy on continuous carbon film grids for 15 min to reach a TEM sample thickness of ~150 nm. Bright-field imaging was performed using a Tecani F20 TEM operated at 200 kV with a field emission gun. After the tensile testing, the surface of the fractured samples was investigated using scanning electron microscopy (SEM, Hitachi SU-70 at 20 kV). Selected samples were also investigated from the cross-sections right below the surface crack. The cross-sectional samples were prepared by focused ion beam microscopy (FEI Quanta 200 3D) in the direction perpendicular to the surface crack. A square area was first milled at a high Ga^+ current density. During the final milling steps, reduced current densities was applied to achieve a smooth milling area below the surface.

Tensile testing of the system was performed following procedures described before [4]. Briefly, quasi-static tensile test at constant strain rate of $4 \times 10^{-4} s^{-1}$ was carried out with $\sim 4 \times 20\ mm^2$ gauge area. Strain was measured in-situ using digital image correlation (DIC) methods, as shown in Fig. 1 (a). The critical strain ε_c was determined by electrical resistance change method.

2.2. Finite element simulations

The finite element simulations were carried out using ANSYS APDL. A 2D plane-strain model was constructed, similar to those in [16–18,30,31] and verified by the results in [16]. The thickness of the metallic film, buffer layer, and PI substrate was taken from experimental measurements, and the width of the whole system was set to be 3.12 μm. Simulations were performed for samples on either smooth or rough (100 nm R_a) PI substrate with Al or Cr buffer layer of 20–100 nm. To simulate fracture, the cohesion zone model (CZM) [32] was implemented in this work using ANSYS APDL codes. An exponential law was used here to describe the separation of two material surfaces [32]. The critical stress for crack initiation was taken as the yield or fracture stress of the material considered [33], i.e. Al, Cr and Al-Mn used in the current work. The normal and shear separation across the interface, were assumed to be identical and obey the fracture energy law [16,34]. The film/buffer layer interface was modeled to be well bonded. The whole system was meshed by the 2D 8-node structural solid element (Plane183) under plane strain and the interfaces were meshed by the 6-node cohesive element Inter203. Convergence analysis was performed with the mesh to get the mesh-independent results.

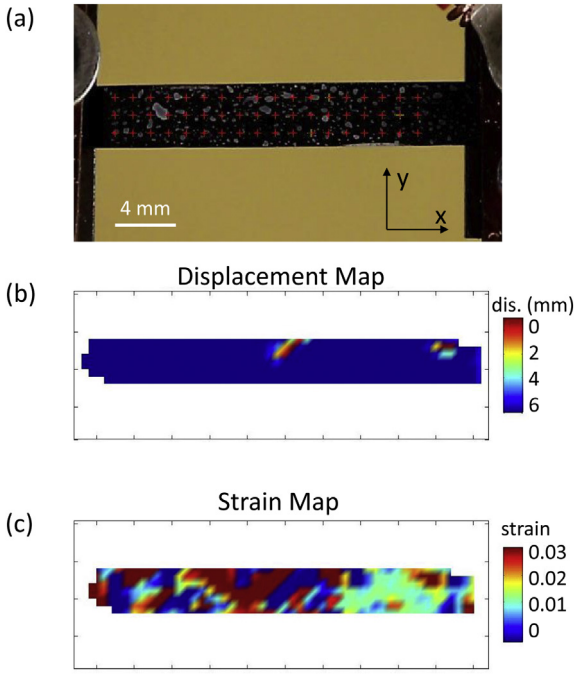

Fig. 1. (a) Sample with ink sprayed on its surface for DIC analysis and the grid generated by the DIC code, and the corresponding (b) displacement and (c) strain map of sample in (a) at the time when the critical strain occurs. Tensile stress was applied in the x direction.

3. Results

3.1. Microstructure and mechanical property of Al-Mn/PI

Microstructure of the as-deposited Al-Mn thin films was characterized by TEM prior to mechanical testing. HRTEM in Fig. 2(a) shows a completely amorphous phase was present and no long-range order was detected in the whole film, similar to those observed in electrodeposited Al-Mn films with similar composition [35]. The amorphous nature of the film is also confirmed by the diffuse halo in the SAD pattern (Fig. 2(b)).

The mechanical properties of Al-Mn/PI were evaluated by uniaxial tensile testing and the test was stopped right after the critical strain ε_c is reached, as measured by the electrical resistance change, as shown in Fig. 3. Fig. 1(b) and (c) shows the displacement and strain distribution respectively of the whole sample measured by DIC at ε_c. It can be seen that while the displacement was relatively uniform, large variations of local strain, from 0 to 3% can be seen on the sample. Fig. 4 shows a representative true stress-strain curve of a monolithic Al-Mn alloy

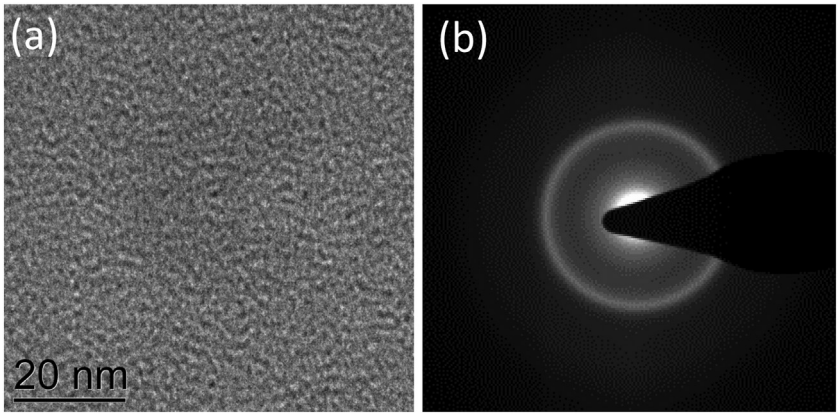

Fig. 2. (a) HRTEM image and (b) corresponding SAD pattern of as-deposited monolithic Al-Mn film.

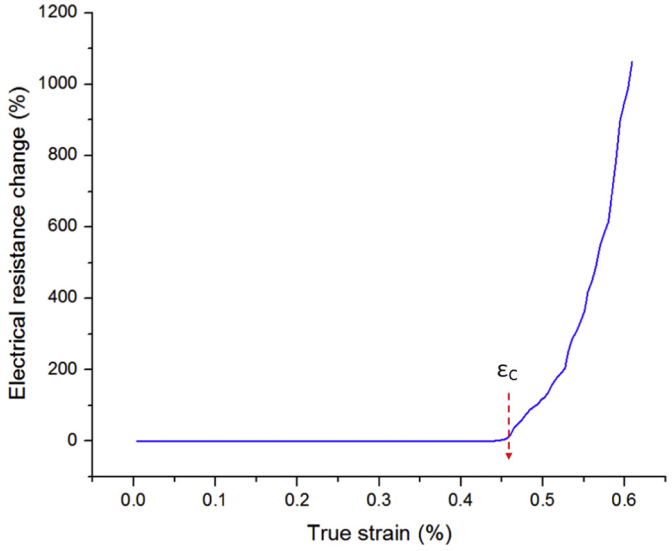

Fig. 3. Evolution of electrical resistance change (defined as $(R-R_0)/R_0$, where R_0 is the initial electrical resistance of the film) of a monolithic Al-Mn (sample M) as a function of strain. The arrow indicates critical strain ε_c.

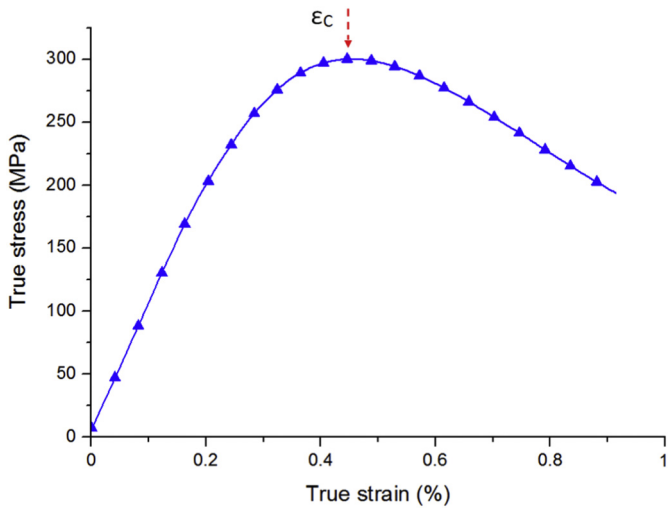

Fig. 4. Representative true stress-strain curve of sample M. The arrow indicates critical strain ε_c.

Table 1
Composition and mechanical properties of monolithic Al-Mn thin film. The critical strain (ε_c) was obtained from electrical resistance change method while fracture stress (σ_f) and elastic modulus (E) were measured from uniaxial tensile tests experimentally. The Poisson's ratio (ν) was estimated using the rule of mixtures from pure Al and Mn [36].

Alloy	ε_c (%)	σ_f (MPa)	ν	E (GPa)
Al-Mn	0.46 ± 0.01	321.7 ± 22.7	0.32	103.6 ± 2.9

sample, from which the mechanical properties of the Al-Mn alloy including fracture stress (σ_f) and elastic modulus (E) were extracted (listed in Table 1) and used for finite element analysis (FEA) afterwards. Once the experiments were ended, extensive cracks were observed on the specimen, mostly perpendicular to the loading direction, as shown in Fig. 5 (a). Selected samples were also milled by focus ion beam from the cross-sections, as shown in Fig. 5(b). It can be seen that in addition to the through-thickness crack within the amorphous Al-Mn film, small cracks at the film/substrate interface can also be detected.

To investigate the effects of the PI substrate roughness and the buffer layer type on the thin film/substrate adhesion, tensile tests were conducted on un-buffered and buffered Al-Mn|PI films with either smooth or rough PI substrates (listed in Table 2). In the buffered samples, a 20 nm thick Cr layer was deposited between the Al-Mn thin film and the PI substrate. Table 2 summarizes the experimentally measured critical strains for all samples after tensile tests (following the procedure described earlier), except for sample sets C. The film/substrate adhesion of sample C was too weak that the film delaminated whenever it was in contact with hands. It can be seen that at the absence of the buffer layer, enhancing surface roughness alone from sample sets A to B enhanced the critical strain of the system from 0.46% to 1.39%. By adding a buffer layer on a rough substrate, the overall critical strain of the brittle metal/PI system was significantly increased from 0.46% (sample sets A) to 4.66% (sample sets D).

3.2. FEA study

The material properties used in the FEA are summarized in Table 3. The properties of the Al-Mn film were obtained experimentally (Table 1). The properties of the PI were obtained directly from the manufacturer, Dupont Kapton® (Table 3). The yield strength of Al thin film (of 1 μm) was obtained experimentally in this study by nanoindentation and the fracture stress of Cr thin film (of 50 nm) was obtained from reference [37]. The elastic moduli and Poisson's ratios of Al and Cr are assumed to be similar to bulk properties and were obtained from reference [36]. All the metallic materials were assumed to follow an elastic-perfectly plastic behavior using either σ_y or σ_f as the flow stress.

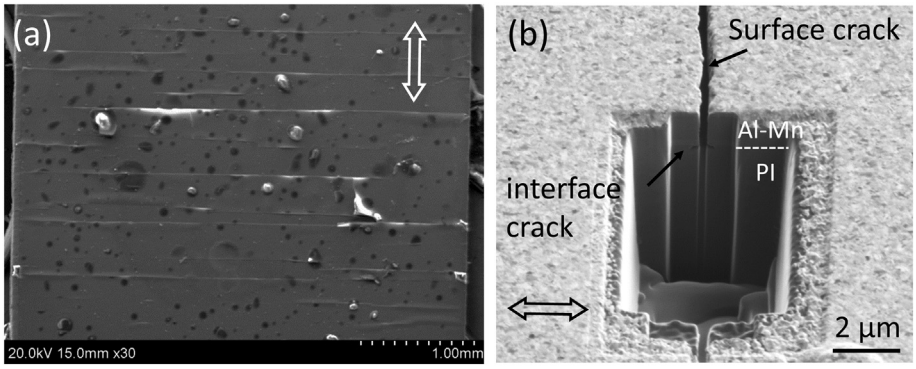

Fig. 5. (a) Typical surface and (b) cross-sectional SEM images of amorphous Al-Mn/PI after tensile testing right after reaching critical strain. The double-arrows in both images indicate the loading direction.

CZM was implemented here to simulate fracture of the system. It is well known that the traditional linear elastic fracture mechanics approaches cannot predict crack nucleation. When the plastic zone size around the crack tip becomes comparable to or larger than the characteristic size, which is known as the idealized radius of the plastic zone of deformation at the crack tip [38], the small plastic zone size assumption is no longer valid thus requiring an alternative approach. CZM, on the other hand, allows the investigation of both crack nucleation and growth during interfacial delamination. Moreover, unlike in other methods, where the presence of a pre-crack is needed (even for brittle materials), this step is not required when using CZM. Therefore, instead of introducing an imperfection (e.g. V-shaped notch) where the crack can nucleate [16,18,30], in this work, cohesive zones were defined around a through-thickness zone of the film and at the interface between the film and the PI substrate, without any special geometry assumption, as shown in Fig. 6.

To investigate the adhesion of the interface between two dissimilar, non-linear elastic materials (i.e. the film/PI system), path-independent J-integral has been proven to be the only feasible computational method [39–41]. Recently, some authors have investigated the adhesion of multilayer metallic films coated on PI substrates with an approach based on a buckling model [42–46]. However, this approach cannot be directly applied to flexible systems in which there contain at least one brittle layer and a polymer substrate. Specifically, the buckling model approach assumes no cracking or plastic deformation in the film or substrate during buckling, and the adhesion energy was determined at a high critical buckling strain (e.g. > 13%) [42]. Those assumptions cannot be applied here because at such large strain, the brittle layer (or film) would have cracked and the PI substrate plastically deformed.

If a monotonic loading is assumed (i.e. without any plastic unloading), J-integral can be defined as a path-independent line integral which measures the strength of the singular stress and strain field near the crack tip. In a nonlinear elastic structure that contains a crack, the J integral is defined as [41]

$$J = \int_{\Gamma} wdy - T_i \frac{\partial u_i}{\partial x} ds \quad (1)$$

where $w = \int_0^{\varepsilon_{ij}} \sigma_{ij} d\varepsilon_{ij}$ is the strain energy density, $T_i = \sigma_{ij} n_j$ is the traction vector, Γ is an arbitrary contour around the tip of the crack, n is the unit vector normal to Γ, and σ, ε, u are the stress, strain, and displacement fields, respectively.

Table 3
Summary of material properties used in FEA simulations.

Material	E (GPa)	ν	σ_y (MPa)	σ_f (MPa)
PI	2.5	0.34	69	–
Al	70.2	0.345	225.4	–
Cr	279	0.21	–	1618.2

As described in the ANSYS documentation, the strain energy density w can be preferably defined per element. That means it is possible to divide the strain energy for each element. Creating a path around the crack tip, mapping the strain energy density on this path and integrate over the path length with respect to y, gives the first term $\int_\Gamma w dy$. Defining a normal vector to the path Γ and using the stresses σ_x, σ_y and σ_{xy} makes it possible to get the traction vector $T_i = \sigma_{ij} n_j$ working on the path. The derivatives $\frac{\partial u_i}{\partial x}$ are defined by mapping the displacements to the path, then moving the path a distance in the x-direction in the local crack tip coordinate system. Knowing the distance ∂x and the path it is moved makes it possible to approximate the derivatives. With the traction vector and the derivatives of the displacements known, the second term $\int_\Gamma T_i \frac{\partial u_i}{\partial x} ds$ in Eq. (5) can be calculated. J-integral has been implemented in ANSYS in such four steps, where the J- integral is calculated at the solution phase of the analysis. Once each sub-step has converged, the software stores the values in the results file. Here a strain of 4.66% (i.e. critical strain of sample D, Table 2) was applied to all samples. Twelve contours were defined around the crack tip, which rested at the film/substrate interface, until the J-integral values converged. The singularity around which the J-integral is calculated in the first place is the intersection between the vertical and the horizontal cohesive zones (crack tip as shown in Fig. 6).

To model the rough PI samples, a FEM model of a buffered system with rough PI substrate was constructed. For simplicity, the film/PI interface was assumed to be wavy with sinusoidal shape as

$$y = a \sin \frac{2\pi}{\lambda} x \quad (2)$$

Table 2
Summary of composition, substrate surface roughness (R_a), Cr buffer layer thickness (h_{Cr}), and critical strain (ε_c) of all sample sets measured experimentally. All experimental measurements were obtained from at least three separate tests. J-integral values were obtained from FEA simulations.

Sample ID	Film composition	PI R_a (nm)	$h_{Al\text{-}Mn}$ (nm)	h_{Cr} (nm)	ε_c (%)	J-integral (J/m^2)
A	Al-Mn|PI	–	1200	–	0.46 ± 0.01	0.69
B	Al-Mn|PI	100 ± 6	1200	–	1.39 ± 0.1	1.82
C	Al-Mn|Cr|PI	–	1180	20 ± 5	–	0.96
D	Al-Mn|Cr|PI	100 ± 6	1180	20 ± 5	4.66 ± 0.1	8.93

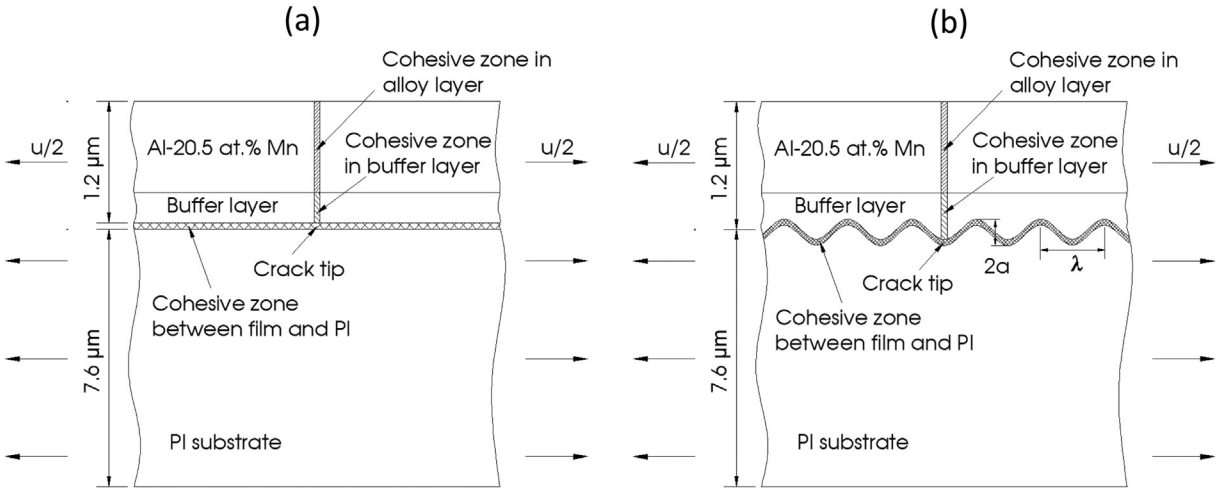

Fig. 6. Schematic sketch of a buffered sample with through-thickness (vertical) and interfacial (horizontal) cohesive zones on a (a) smooth and (b) rough PI substrate.

where a is the amplitude, λ is the wavelength and x is the horizontal displacement. For the roughness R_a of 100 nm, λ and a in Fig. 6(b) take the values of 2 μm and 100 nm, respectively. The length l of the model was set to be equal to 2λ, i.e. two sinusoidal periods. The nominal strain of the system was then $u/l = u/(2\lambda)$.

Different from the model in reference [26] where the film was simulated to be bonded to the wavy PI substrate, in this work the cohesive zones were introduced both inside the metal layers (through thickness) as well as at the film/substrate interface, similar to the above mentioned smooth surface model. All the other geometry, material parameters, and boundary conditions were the same as the smooth surface model. Table 4 summarizes all the J-integral results obtained from FEA. Comparing the simulation results with the experiments, Table 2 shows the trend between the experimentally-measured critical strains matches well with the simulated J-integrals. Therefore, it is expected that the measured critical strains strongly correlate with the film/substrate adhesion (hence, J-integrals) [39–41]. In summary, both experimental and simulation results indicate that the combination of a buffer layer and rough substrate dramatically enhanced the film/substrate adhesion and delayed the system failure.

4. Discussions

Fig. 7 shows simulated J-integrals of M, MAl20, and MCr20 samples (as defined in Table 4) on smooth and rough PI substrate. It can be seen that for all samples on smooth substrate, the one with Al buffer layer (MAl20) has the highest J-integral value, hence interface adhesion. This can be rationalized by the stress and strain distribution of the film/PI system, and the extent of substrate plastic deformation. First, comparing MAl20 and MCr20 samples, higher equivalent stress is distributed broadly in the Al-Mn alloy layer of MAl20 (Fig. 8(a)), with the maximum value of about 200 MPa. Meanwhile the stress concentrates in the buffer layer of Cr (20 nm) with a maximum value of ~901 MPa in MCr20 (Fig. 8(b)). This stress concentration in the Cr layer obviously creates a higher traction at the interface, increasing the possibility of delamination. That is likely the reason why the interfacial adhesion of MAl20 is about three times higher than that of MCr20. Secondly, it can be seen that there is no yielding in Al layer in MAl20 (since the equivalent stress in the Al layer is much lower than its yield strength, shown in Fig. 8(a)) while all the PI substrates yielded. The plastic strain distribution in sample MAl20 (Fig. 8(c)) shows a high plastic strain concentration (about 31%) near crack tip in the PI substrate while in MCr20 (Fig. 8(d)) there is only about 5% of plastic strain near crack tip within the PI substrate. According to Was et al. [20], the plastic deformation has a significant impact on the toughness of the interface in a multilayer system. A tough interface is attributed to extensive plastic work done at the crack tip during crack propagation. The substrate PI in MAl20 sample clearly shows the highest plastic deformation among the smooth substrate samples. Based on the above discussions, it can be postulated that, to improve the interface toughness of a brittle film on a smooth flexible PI substrate, a ductile buffer layer with smaller yield/fracture strength than the brittle film (e.g. Al for Al-Mn) should be added in between the film and the substrate. This way, the yield/fracture strength of the system gradually increases from the substrate to the amorphous thin film, with the added buffer layer distribute the stress more uniformly along the film/substrate interface, providing better 'glue' effect.

Fig. 9 summarizes the effects of buffer layer thickness on the interface adhesion of all samples. It can be seen that the substrate roughness takes its best effect on the adhesion with Cr (instead of Al) buffer layer. In addition, while the J-integral values of MAlx and MAlx-R (x = 20, 50, 75 and 100 nm) samples is almost insensitive to buffer layer thicknesses, that of MCrx and MCrx-R samples reaches the maximum at x = 75 nm. This different buffer layer thickness dependence is mainly due to the difference in strength between Al and Cr buffer layer. As shown in Fig. 8(a), the equivalent stress in the Al layer is much lower than its yield strength, meaning that there is no yielding in the Al layer in MAl20, while the PI substrate yielded (the same is observed in all the MAlx and MAlx-R samples, results not shown here). Therefore, the elastic energy absorbed by the Al layers (20, 50, 75 and 100 nm) is quite small compared to that by the Cr layers. In other words, the Al layers (regardless of the roughness) dissipate a rather small amount of strain energy. Hence the interfacial adhesion of the system does not vary much with respect to the Al layer thickness. Here we will focus on the most beneficial case, sample MCr75-R, which improves the interface toughness of the base sample M by almost 20 times. By systematically increasing the thickness of the Cr film, the combined elastic energy stored in the two adjacent layers increases, making it higher than the critical condition sufficient to delaminate the interface [47]. It was found that the Cr layers in MCr75 and MCr75-R possess the highest values of elastic energy density compared to other MCrx and MCrx-R (x = 20, 50 and 100 nm), respectively. From Fig. 11, it can be seen that at the same critical strain, the energy is absorbed more by the thicker Cr layers until the maximum energy absorption ability is reached at x = 75 nm in MCr75-R. In other words, the Cr layers of 75 nm dissipate the highest amount of strain energy, increasing the ability of preserving ductility and delaying the final failure of the whole system, similar to that reported in [48].

It has been shown that interface toughness can be improved by roughening the substrate [23,49]. Results in Fig. 7 demonstrate that

Table 4
Summary of substrate surface roughness (R_a), buffer layer material type and thickness (h_{buffer}) of all samples studied using FEA simulations. The brittle metallic film used for all samples has a composition of Al-20.5 at.% Mn. The J-integral for all samples was calculated from FEA simulation at a tensile strain of 4.66%, as determined experimentally from sample sets D in Table 2.

Sample ID	R_a (nm)	Buffer layer	h_{Al-Mn} (nm)	h_{buffer} (nm)	J-integral (J/m^2)
M	-	-	1200	-	0.69
M-R	100	-	1200	-	1.82
MAl20	-	Al	1180	20	3
MAl50	-	Al	1150	50	2.97
MAl75	-	Al	1125	75	2.98
MAl100	-	Al	1100	100	3.02
MAl20-R	100	Al	1180	20	5.97
MAl50-R	100	Al	1150	50	5.15
MAl75-R	100	Al	1125	75	4.9
MAl100-R	100	Al	1100	100	4.75
MCr20	-	Cr	1180	20	0.96
MCr50	-	Cr	1150	50	2.65
MCr75	-	Cr	1125	75	3.54
MCr100	-	Cr	1100	100	2.92
MCr20-R	100	Cr	1180	20	8.93
MCr50-R	100	Cr	1150	50	12.26
MCr75-R	**100**	**Cr**	**1125**	**75**	**13.62**
MCr100-R	100	Cr	1100	100	12.18

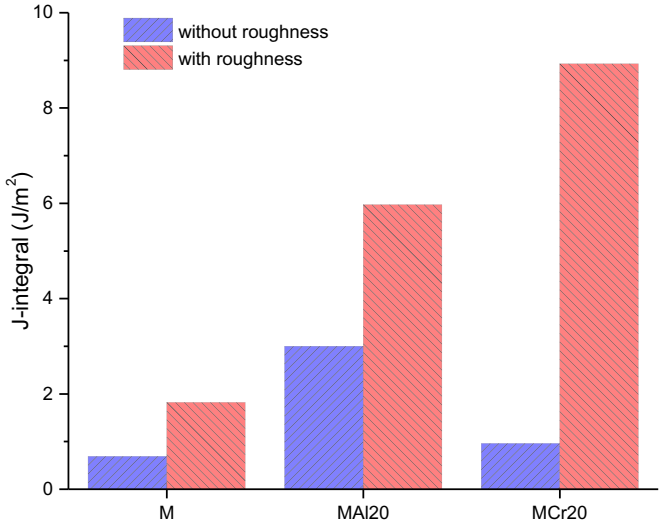

Fig. 7. FEA simulation results of J-integrals of sample M, M-R, MAl20, MAl20-R, MCr20 and MCr20-R, as defined in Table 3.

rough PI substrate can improve the interface toughness within the three samples (M, MAl20 and MCr20). J-integral values of M-R and MAl20-R samples have nearly doubled with the presence of substrate roughness. In MCr20-R, the interfacial adhesion increased nine times compared with the smooth substrate sample MCr20. Moreover, the interfacial adhesion of MCr20-R is about 5 and 1.5 times respectively in comparison with its counterparts, i.e. M-R and MAl20-R. Note that similar to MAl20, there is no yielding in the Al layer of MAl20-R. Hence the fracture of all six samples fall into the debonding mechanism as categorized in reference [20]. Dauskardt, Lane, Ma and Krishna [23] showed that energy dissipation during the debonding was affected by the interface morphology due to the increase in frictional sliding of the surface asperities behind the debonding tip. A model in [50] also shows that the increased adhesion of a rough interface results from the extension of the frictional contact zone behind the debonding tip. Secondly, rough interface can reduce the tensile stresses along the film surface, thus restraining the channel cracking of the film as well as the debonding [26]. Lastly, high energy dissipation of the film by plastic deformation on rough substrate could be considered as a toughening mechanism that contributes to the enhanced interface toughness [23]. The energy dissipation mechanism involves the plastic deformation of the ductile bonding layer(s) and the interaction between the crack faces

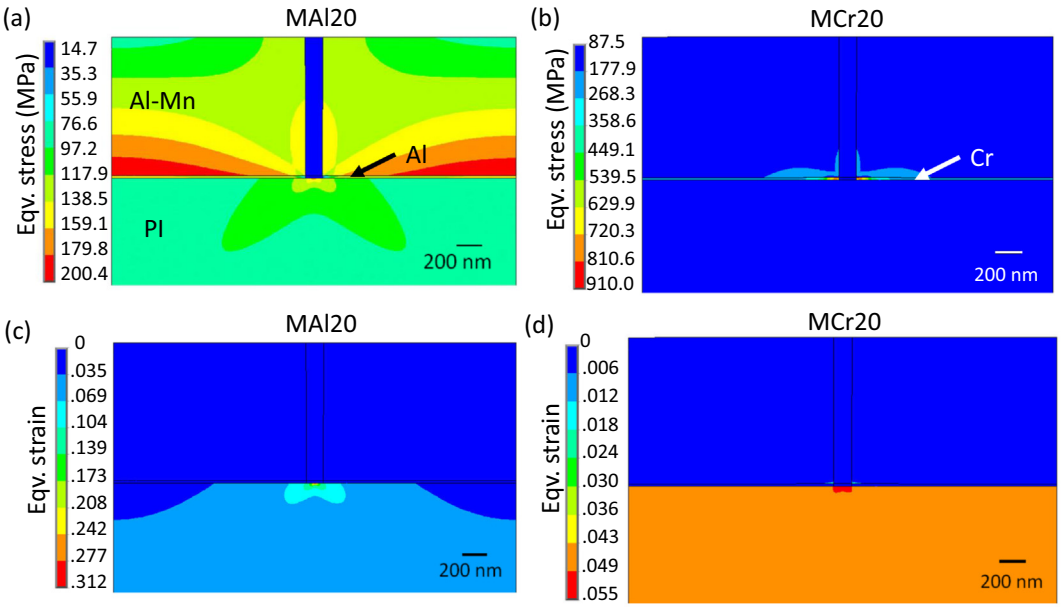

Fig. 8. FEA simulation results of (a), (b) equivalent stress (MPa) and (c), (d) plastic equivalent strain distributions of sample MAl20 and MCr20 after 4.66% tensile strain loading.

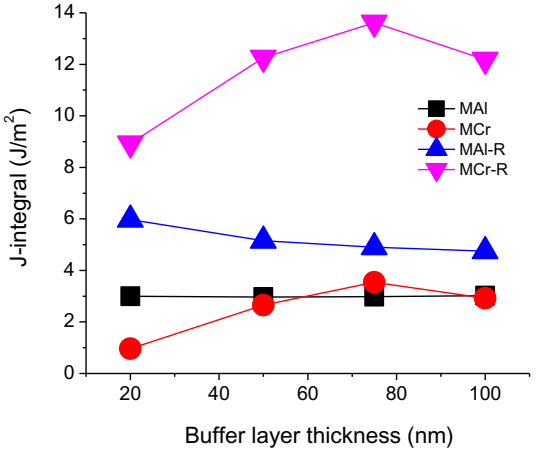

Fig. 9. Summary of FEA simulation results of J-integrals as a function of the buffer layer thicknesses for all samples.

behind the debonding tip. Fig. 10 shows the plastic strain energy densities of the buffered rough samples. It can be seen that the plastic strain energy density of the PI substrate in MCr20-R is two times that of MAl20-R. That means the energies stored in the films dissipated by the substrate in MCr20-R is more than that of MAl20-R, making the interface toughness in MCr20-R higher. Therefore, it is postulated that with the rough PI substrate, higher adhesion of an amorphous brittle film/PI interface can be obtained by having a buffer layer with higher strength and stiffness. Lastly, it should also be noted that whether an optimum substrate roughness exist for the highest interface roughness is still unknown, which is left for future work.

5. Conclusions

Through combined experiments and FEA, it was found that the interface toughness of amorphous Al-Mn alloy thin films coated on PI substrates could be improved by adding buffer layer (Al or Cr) and roughening the substrates. At a fixed buffer layer thickness (20 nm) on smooth substrate, system with Al buffer layer exhibited interfacial adhesion three times higher than that with Cr layer. This was mainly attributed to the fact that Al (unlike Cr) has a smaller yield strength than amorphous Al-Mn, thus distributing the stress more uniformly along the film/substrate interface, providing better enhancement of interface toughness. On the other hand, introducing substrate roughness enhanced interfacial adhesion of all samples, with the most significant enhancement for systems with Cr buffer layer. An optimum Cr layer thickness of 75 nm was identified. At this thickness, the highest amount of strain energy dissipation ability was reached, maximizing the ability of preserving ductility and delaying the final failure of the whole system. The results of the present work may shed light on the interfacial

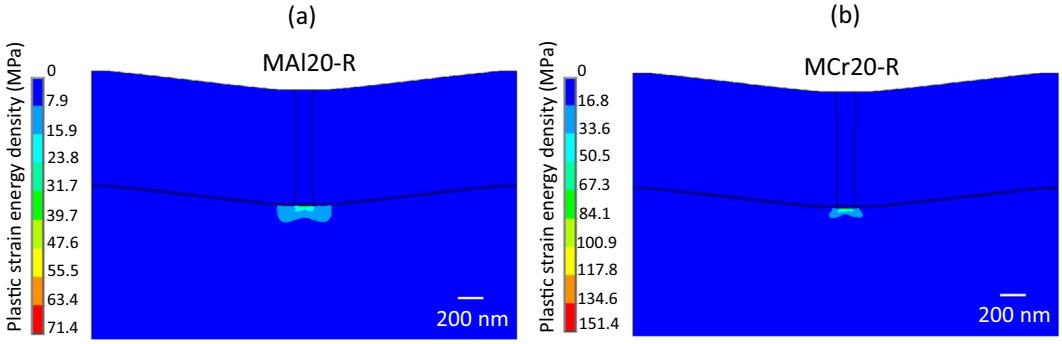

Fig. 10. FEA simulation results of plastic strain energy densities (MPa) of (a) MAl20-R and (b) MCr20-R after 4.66% tensile strain loading.

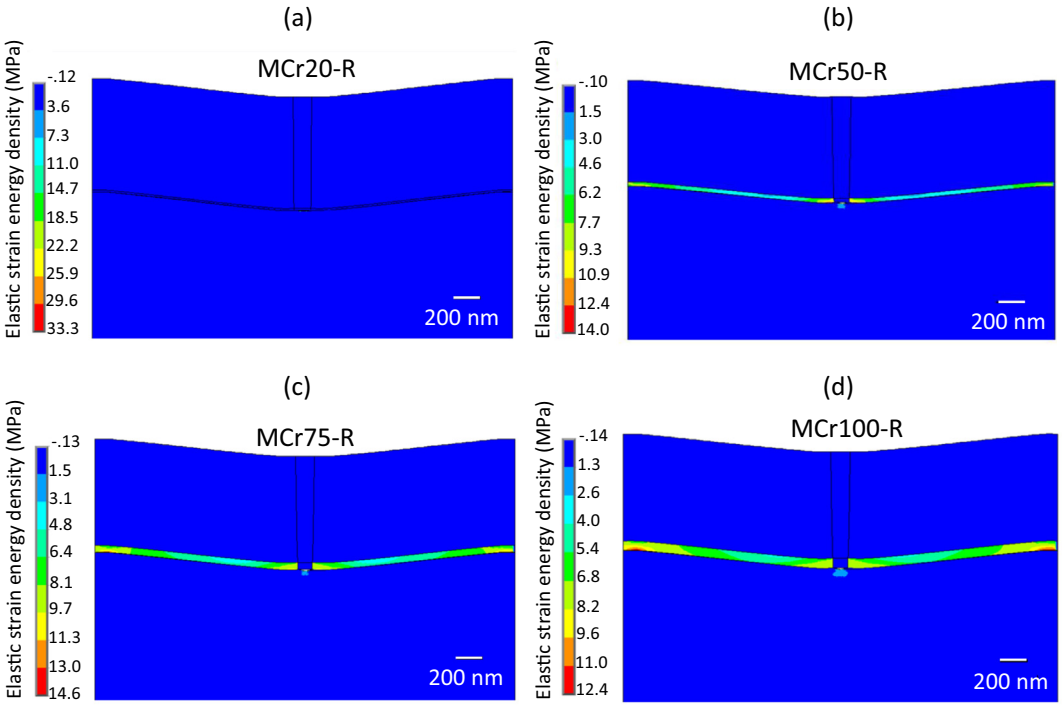

Fig. 11. FEA simulation results of elastic strain energy densities (MPa) of the rough samples with Cr buffer layers (a) MCr20-R, (b) MCr50-R, (c) MCr75-R and (d) MCr100-R after 4.66% tensile strain loading.

engineering strategies for improving interface toughness for flexible electronics, whose reliable performance requires enhanced interface toughness of brittle thin films on polymer substrates.

Acknowledgments

The sample preparation and materials characterization were performed at the Nano Research and Educational Center (NREC) at the University of South Florida. H.T. acknowledges support by the Vietnamese Ministry of Education and Training's fund for Vietnamese scholars overseas. H.T. and W. C. thankfully acknowledge the financial support by the National Science Foundation under Grant DMR-1856196 and CMMI-1855651.

References

[1] T. Egami, P.J. Flanders, C.D.G. Jr, Amorphous alloys as soft magnetic materials, AIP Conf. Proc. 24 (1) (1975) 697–701.
[2] Y.Q. Cheng, H.W. Sheng, E. Ma, Relationship between structure, dynamics, and mechanical properties in metallic glass-forming alloys, Phys. Rev. B 78 (1) (2008) 014207.
[3] R. Vaidyanathan, M. Dao, G. Ravichandran, S. Suresh, Study of mechanical deformation in bulk metallic glass through instrumented indentation, Acta Mater. 49 (18) (2001) 3781–3789.
[4] H.T. Tran, H. Mraied, S. Izadi, A.A. Volinsky, W.J. Cai, Optimizing ductility and fracture of amorphous metal thin films on polyimide using multilayers, Int. J. Fract. 204 (2) (2017) 129–142.
[5] M.E. McHenry, M.A. Willard, D.E. Laughlin, Amorphous and nanocrystalline materials for applications as soft magnets, Prog. Mater. Sci. 44 (4) (1999) 291–433.
[6] M. Phan, H. Peng, Giant magnetoimpedance materials: fundamentals and applications, Prog. Mater. Sci. 53 (2) (2008) 323–420.
[7] T.P. Moffat, G.R. Stafford, D.E. Hall, Pitting corrosion of electrodeposited aluminum-manganese alloys, J. Electrochem. Soc. 140 (10) (1993) 2779–2786.
[8] J.P. Chu, J.C. Huang, J.S.C. Jang, Y.C. Wang, P.K. Liaw, Thin film metallic glasses: preparations, properties, and applications, JOM 62 (4) (2010) 19–24.
[9] H. Mraied, W. Cai, A. Sagüés, Corrosion resistance of Al and Al–Mn thin films, Thin Solid Films 615 (2016) 391–401.
[10] W.H. Wang, Bulk metallic glasses with functional physical properties, Adv. Mater. 21 (45) (2009) 4524–4544.
[11] C.W. Chu, J.S.C. Jang, S.M. Chiu, J.P. Chu, Study of the characteristics and corrosion behavior for the Zr-based metallic glass thin film fabricated by pulse magnetron sputtering process, Thin Solid Films 517 (17) (2009) 4930–4933.
[12] A. Inoue, Bulk amorphous and nanocrystalline alloys with high functional properties, Mater. Sci. Eng. A 304–306 (0) (2001) 1–10.
[13] L. Tian, Y.-Q. Cheng, Z.-W. Shan, J. Li, C.-C. Wang, X.-D. Han, J. Sun, E. Ma, Approaching the ideal elastic limit of metallic glasses, Nat. Commun. 3 (2012) 609.
[14] Y. Xiang, T. Li, Z.G. Suo, J.J. Vlassak, High ductility of a metal film adherent on a polymer substrate, Appl. Phys. Lett. 87 (16) (2005) 161910.
[15] M. George, C. Coupeau, J. Colin, J. Grilhe, Mechanical behaviour of metallic thin films on polymeric substrates and the effect of ion beam assistance on crack propagation, Acta Mater. 53 (2) (2005) 411–417.
[16] Z. Zhang, T. Li, Effects of grain boundary adhesion and grain size on ductility of thin metal films on polymer substrates, Scr. Mater. 59 (8) (2008) 862–865.
[17] T. Li, Z.Y. Huang, Z.C. Xi, S.P. Lacour, S. Wagner, Z. Suo, Delocalizing strain in a thin metal film on a polymer substrate, Mech. Mater. 37 (2–3) (2005) 261–273.
[18] T. Li, Z. Suo, Ductility of thin metal films on polymer substrates modulated by interfacial adhesion, Int. J. Solids Struct. 44 (6) (2007) 1696–1705.
[19] N. Lu, X. Wang, Z. Suo, J. Vlassak, Failure by simultaneous grain growth, strain localization, and interface debonding in metal films on polymer substrates, J. Mater. Res. 24 (02) (2009) 379–385.
[20] G.S. Was, T. Foecke, Deformation and fracture in microlaminates, Thin Solid Films 286 (1–2) (1996) 1–31.
[21] G.R. Odette, B.L. Chao, J.W. Sheckherd, G.E. Lucas, Ductile phase toughening mechanisms in a TiAl TiNb laminate composite, Acta Metall. Mater. 40 (9) (1992) 2381–2389.
[22] M.Y. He, F.E. Heredia, D.J. Wissuchek, M.C. Shaw, A.G. Evans, The mechanics of crack growth in layered materials, Acta Metall. Mater. 41 (4) (1993) 1223–1228.
[23] R.H. Dauskardt, M. Lane, Q. Ma, N. Krishna, Adhesion and debonding of multi-layer thin film structures, Eng. Fract. Mech. 61 (1) (1998) 141–162.
[24] A. Misra, J.P. Hirth, R.G. Hoagland, Length-scale-dependent deformation mechanisms in incoherent metallic multilayered composites, Acta Mater. 53 (18) (2005) 4817–4824.
[25] S. Frank, U.A. Handge, S. Olliges, R. Spolenak, The relationship between thin film fragmentation and buckle formation: synchrotron-based in situ studies and two-dimensional stress analysis, Acta Mater. 57 (5) (2009) 1442–1453.
[26] W. Xu, J.S. Yang, T.J. Lu, Ductility of thin copper films on rough polymer substrates, Mater. Des. 32 (1) (2011) 154–161.
[27] Y.S. Lin, H.M. Liu, Enhanced adhesion of plasma-sputtered copper films on polyimide substrates by oxygen glow discharge for microelectronics, Thin Solid Films 516 (8) (2008) 1773–1780.
[28] C.A. Schuh, T.C. Hufnagel, U. Ramamurty, Mechanical behavior of amorphous alloys, Acta Mater. 55 (12) (2007) 4067–4109.
[29] I.S. Park, J. Yu, An X-ray study on the mechanical effects of the peel test in a Cu/Cr/polyimide system, Acta Mater. 46 (8) (1998) 2947–2953.
[30] N. Lu, Z. Suo, J.J. Vlassak, The effect of film thickness on the failure strain of polymer-supported metal films, Acta Mater. 58 (5) (2010) 1679–1687.
[31] T. Li, Z. Huang, Z. Suo, S.P. Lacour, S. Wagner, Stretchability of thin metal films on elastomer substrates, Appl. Phys. Lett. 85 (16) (2004) 3435–3437.
[32] K. Park, G.H. Paulino, Cohesive zone models: a critical review of traction-separation relationships across fracture surfaces, Appl. Mech. Rev. 64 (6) (2013) 060802.
[33] D.S. Dugdale, Yielding of steel sheets containing slits, J. Mech. Phys. Solids 8 (2)

(1960) 100–104.
[34] W. Xu, T.J. Lu, F. Wang, Effects of interfacial properties on the ductility of polymer-supported metal films for flexible electronics, Int. J. Solids Struct. 47 (14–15) (2010) 1830–1837.
[35] S.Y. Ruan, C.A. Schuh, Electrodeposited Al-Mn alloys with microcrystalline, nanocrystalline, amorphous and nano-quasicrystalline structures, Acta Mater. 57 (13) (2009) 3810–3822.
[36] F. Cardarelli, Materials Handbook: A Concise Desktop Reference, Springer–Verlag, London, 2008.
[37] M.J. Cordill, A. Taylor, J. Schalko, G. Dehm, Fracture and delamination of chromium thin films on polymer substrates, Metall. Mater. Trans. A 41A (4) (2010) 870–875.
[38] G.R. Irwin, Analysis of stresses and strains near the end of a crack traversing a plate, J. Appl. Mech. 24 (1957) 361–364.
[39] H.T. Tran, M.H. Shirangi, X. Pang, A.A. Volinsky, Temperature, moisture and mode-mixity effects on copper leadframe/EMC interfacial fracture toughness, Int. J. Fract. 185 (1) (2013) 115–127.
[40] J.R. Rice, G.C. Sih, Plane problems of cracks in dissimilar media, J. Appl. Mech. 32 (2) (1965) 418–423.
[41] T.L. Anderson, Fracture Mechanics: Fundamentals and Applications, CRC Press, Boca Raton, Florida, USA, 2005.
[42] M.J. Cordill, F.D. Fischer, F.G. Rammerstorfer, G. Dehm, Adhesion energies of Cr thin films on polyimide determined from buckling: experiment and model, Acta Mater. 58 (16) (2010) 5520–5531.
[43] V.M. Marx, C. Kirchlechner, I. Zizak, M.J. Cordill, G. Dehm, Adhesion measurement of a buried Cr interlayer on polyimide, Philos. Mag. 95 (16–18) (2015) 1982–1991.
[44] K. Wu, J.Y. Zhang, G. Liu, P. Zhang, P.M. Cheng, J. Li, G.J. Zhang, J. Sun, Buckling behaviors and adhesion energy of nanostructured Cu/X (X = Nb, Zr) multilayer films on a compliant substrate, Acta Mater. 61 (20) (2013) 7889–7903.
[45] K. Wu, J.Y. Zhang, J. Li, Y.Q. Wang, G. Liu, J. Sun, Length-scale-dependent cracking and buckling behaviors of nanostructured Cu/Cr multilayer films on compliant substrates, Acta Mater. 100 (2015) 344–358.
[46] M.J. Cordill, A.A. Taylor, Thickness effect on the fracture and delamination of titanium films, Thin Solid Films 589 (2015) 209–214.
[47] Y. Wei, J.W. Hutchinson, Nonlinear delamination mechanics for thin films, J. Mech. Phys. Solids 45 (7) (1997) 1137–1159.
[48] H. Kou, J. Lu, Y. Li, High-strength and high-ductility nanostructured and amorphous metallic materials, Adv. Mater. 26 (31) (2014) 5518–5524.
[49] Q. Ma, H. Fujimoto, P. Flinn, V. Jain, F. Adibi-Rizi, F. Moghadam, R.H. Dauskardt, Quantitative measurement of interface fracture energy in multi-layer thin film structures, MRS Proc. 391 (1995) 91.
[50] A.G. Evans, J.W. Hutchinson, Effects of non-planarity on the mixed mode fracture resistance of bimaterial interfaces, Acta Metall. 37 (3) (1989) 909–916.